Multimodal analysis of neuronal maturation in the developing primate prefrontal cortex

Yu Gao[1]†, Qiping Dong[1]†, Kalpana Hanthanan Arachchilage[1]†, Ryan D. Risgaard[1], Jie Sheng[1,2], Moosa Syed[1], Danielle K. Schmidt[1], Ting Jin[1,2], Shuang Liu[1], Dan Doherty[2], Ian Glass[2], Birth Defects Research Laboratory[2], Jon E. Levine[3,4], Daifeng Wang[1,5,6]*, Qiang Chang[1,7,8]*, Xinyu Zhao[1,3]*, André M. M. Sousa[1,3]*

[1]Waisman Center, University of Wisconsin-Madison; Madison, WI, USA

[2]Department of Pediatrics, University of Washington School of Medicine; Seattle, WA, USA

[3]Department of Neuroscience, University of Wisconsin-Madison; Madison, WI, USA

[4]Wisconsin National Primate Research Center, University of Wisconsin-Madison; Madison, WI 53705

[5]Department of Biostatistics and Medical Informatics, University of Wisconsin-Madison; Madison, WI, USA

[6]Department of Computer Sciences, University of Wisconsin-Madison; Madison, WI, USA

[7]Department of Medical Genetics, University of Wisconsin-Madison; Madison, WI, USA

[8]Department of Neurology, University of Wisconsin-Madison; Madison, WI, USA

†These authors contributed equally to this work.

*Corresponding authors. Email: daifeng.wang@wisc.edu (D.W.), qchang@waisman.wisc.edu (Q.C.), xinyu.zhao@wisc.edu (X.Z.), andre.sousa@wisc.edu (A.M.M.S.)

Abstract: The dorsolateral prefrontal cortex (dlPFC) is a derived cortical area in primates that is involved in myriad high-cognitive functions and is associated with several neuropsychiatric disorders. Here, we performed Patch-seq and single-nucleus multiomic analyses of the rhesus macaque dlPFC to identify genes governing neuronal maturation during midfetal to late-fetal development. Our multimodal analyses have identified genes and pathways important for the maturation of distinct neuronal populations as well as genes underlying the maturation of specific electrophysiological properties. Using gene knockdown in macaque and human organotypic slices, we functionally tested the role of *RAPGEF4*, a gene involved in synaptic remodeling, and *CHD8*, a high-confidence autism spectrum disorder risk gene, on the electrophysiological and morphological maturation of excitatory neurons in the macaque and human fetal dlPFC.

Introduction

The dorsolateral prefrontal cortex (dlPFC), a cortical area highly derived in primates (*1-3*), is critical for myriad higher-order brain functions, including executive functions such as working memory, planning, and decision-making (*3-5*). These functions are significantly impaired in several disorders, including autism spectrum disorders (ASD), schizophrenia, and obsessive-compulsive disorder (*6-8*).

During prefrontal cortical development, after postmitotic excitatory neurons acquire their specific laminar and projection identities, they undergo dynamic morphological and functional maturation governed by intricate gene networks and signaling pathways. Although we have a robust knowledge of the molecular and cellular mechanisms that govern cell specification (*9-15*), and of the mature transcriptomic and electrophysiological properties of neurons in the adult neocortex (*16-19*), our understanding of the gene networks that underlie the early stages of electrophysiological maturation of neurons remains elusive. Therefore, a multimodal profiling of neurons that combines electrophysiological and genomic analyses across midfetal and late-fetal development, a critical period for neuronal maturation, is essential to understand the mechanisms underlying neuronal maturation.

To uncover the molecular mechanisms that underlie the maturation of different cell types in the primate dlPFC, we have performed single-nucleus multiomic (snMultiomic) analyses (snRNA-seq and snATAC-seq of the same nucleus) of the dlPFC from 7 rhesus macaques (*Macaca mulatta)*, from postconceptional day (PCD) 87 to PCD155 (Fig. 1). Furthermore, to infer how changes in gene expression affect the electrophysiological maturation of neurons, we have performed Patch-seq on acute dlPFC slices from 14 macaques, including the same specimens profiled for snRNA-seq and snATAC-seq. This approach allowed us to integrate our electrophysiological analyses with gene expression profiles and to precisely determine the genes that underlie the maturation of specific electrophysiological properties. We have also evaluated the function of selected genes by knocking down their expression in organotypic slices of macaque and human, and evaluating how the loss of function of these genes affects neuronal maturation. This multimodal dataset provides a valuable resource on the primate dlPFC from midfetal to late-fetal development and is accessible at https://daifengwanglab.shinyapps.io/DevMacaquePFC/.

Transcriptomic changes of rhesus macaque dlPFC cells during midfetal and late fetal development

We performed snMultiomic analyses on 7 rhesus macaque dlPFC samples across six prenatal ages: PCD87, PCD96, PCD101, PCD104, PCD112, and two PCD155 (Fig. 1, table S1). After stringent quality control and filtering (Materials and Methods; table S2, figs. S1 and S2), we retained 52,710 nuclei for further analyses (PCD87: 10,709; PCD96: 8,826; PCD101: 5,718; PCD104: 7,622; PCD112: 10,745, PCD155: 9,090). After removing batch effects using the canonical correlation analysis (CCA) based approach (Materials and Methods), we used unsupervised clustering to group nuclei into transcriptomically defined groups (fig. S1B and 1C). Using this strategy, together with cell type-specific marker genes and integration with human and macaque single-cell gene expression datasets (*9, 16, 20*), we defined 9 cell classes that included glutamatergic excitatory neurons, GABAergic inhibitory neurons, glial progenitor cells (GPC), astrocytes, oligodendrocyte precursor cells (OPC), oligodendrocytes, microglia, vascular leptomeningeal cells (VLMC), endothelial cells (Materials and Methods, fig. S2A). We re-clustered the excitatory (ExN) and inhibitory (InN) neuronal nuclei to identify their subclasses, based on the layer (L) and projection identity (intratelencephalic [IT], extratelencephalic [ET], near projecting [NP], corticothalamic [CT], and L6B) for excitatory neurons, and the developmental origin (medial ganglionic eminence [MGE], caudal ganglionic eminence [CGE], or dorsal lateral ganglionic eminence [dLGE]) for inhibitory neurons. We identified 8 ExN subclasses and 3 InN subclasses (Fig. 2B, fig. S2B-C). Interestingly, one population of IT neurons exhibited molecular features of both ExN L2-3 IT and ExN L3-5 IT, possibly indicating that these neurons are yet to be fully specified; we classified this population as ExN L2-3 IT/L3-5 IT. At the lowest hierarchical level of cell type classification, we have transcriptomically defined 74 cell subtypes (table S3 and fig. S2F). By integrating our dataset with two published snRNA-seq datasets that analyzed early fetal (*20*) and adult (*16*) macaque dlPFC, we observed that our data bridges the embryonic/early fetal cell types with the adult cell types, thus facilitating future studies focused on tracing the developmental origins of distinct adult cell subtypes (fig. S3).

As expected, we observed an increasing number of glial cells, including astrocytes, OPCs, and oligodendrocytes throughout late fetal development (Fig. 2C), a period characterized by minimal cortical

neurogenesis and robust gliogenesis (*21*). Within the excitatory neurons, we observed that the intratelencephalic-projecting (IT) neurons were more abundant than any other subclass, as previously described in the adult PFC (*16,17*). The selective expansion of intratelencephalic-projecting neurons in the primate lineage, especially of upper-layer (L2-3) neurons (*16,17*), and their functional relevance in the cortico-cortical circuits that govern some of the unique cognitive and behavioral abilities of primates (*22*), led us to focus our analysis on the maturational profiles of these IT neuronal populations: ExN L2-3 IT and ExN L3-5 IT (Fig. 2D-G). We performed differential gene expression analysis along the developmental trajectory (i.e., pseudotime) to identify genes that display dynamic, highly variable changes during neuronal maturation of ExN L2-3 IT and of ExN L3-5 IT (Materials and Methods). Among the top 250 differentially expressed genes (table S4), we observed genes that exhibit cell type-specific correlation with maturation (Fig. 2E and 2G, fig. S4) and genes that had a conserved maturational expression profile in these two excitatory neuronal populations (Fig. 2H, fig. S4). Among the genes associated with ExN L2-3 IT maturation, we identified *MEIS2*, a transcriptional regulator that is induced by retinoic acid and is important for the arealization of the prefrontal cortex (*23*). Among the genes correlated with ExN L3-5 IT maturation we identified *FOXP2*, a gene encoding a transcription factor that has recently been shown to have a primate-specific expression in L3-5 IT excitatory neurons (*16*). Disruptions in these genes have been linked to neuropsychiatric disorders (*24*). Gene ontology enrichment of the top 250 genes associated with maturation showed that both ExN L2-3 IT and L3-5 IT were enriched for categories such as “cell-cell adhesion”, “neuron projection development”, and “axon development” (Fig. 2I, table S4). However, ExN L2-3 IT were specifically enriched for synaptic related terms, such as “regulation of trans-synaptic signaling” and “modulation of chemical synaptic transmission”, whereas ExN L3-5 IT were enriched for terms related to axonogenesis, such as “neuron projection guidance” and “axon guidance” (Fig. 2I, table S4).

Together, our analyses uncovered the transcriptional landscape of primate midfetal and late fetal prefrontal cortical development, highlighting differences between distinct excitatory neuronal populations throughout maturation.

Chromatin accessibility signature of mid-late fetal dlPFC cells in the rhesus macaque

The simultaneous profiling of gene expression and chromatin accessibility through snMultiomic analysis allows linking putative regulatory elements to genes, thus providing insights into cell-type gene regulatory mechanisms in the developing primate brain. After filtering low-quality nuclei and other stringent quality control steps, snATAC-seq data from 41,822 nuclei were retained for downstream analyses (Materials and Methods; fig. S5A). Using the batch-corrected snATAC-seq data (Materials and Methods, fig. S5B-C), we calculated the UMAP embedding dimensions and observed that the clustering of cells based on accessible chromatin was similar to the clustering utilizing gene expression data (Fig. 3A-B), showing the congruence between the two datasets. However, the snATAC-seq data revealed more pronounced differences in the maturation states of cells within each cell subclass, especially for IT excitatory neurons (fig. S5D).

To gain a better understanding of association of regulatory elements and their target genes during neuronal midfetal and late fetal development, we estimated the peak-to-gene links, which identify co-activity between genes and their nearby accessible chromatin regions (i.e., correlated gene expression values and accessible chromatin peaks across cells), for the excitatory and inhibitory neurons (Materials and Methods, Fig. 3C), thus providing a list of potential regulatory elements for each gene (table S5). We found that peak-gene combinations were hierarchically divided into three distinct categories: a cluster specific to excitatory neurons, a cluster specific to late fetal development, and a cluster specific to inhibitory neurons. Functional enrichment analysis of each group revealed that the cluster specific to late fetal development was enriched for terms such as “negative regulation of EGFR signaling pathway”, “circadian entrainment”, “vesicle-mediated transport in synapse” or “modulation of chemical synaptic transmission” (fig. S6A), processes that indicate the functional maturation of neurons during late fetal development. While genes in the excitatory neuron cluster were enriched for terms such as “neuron projection development”, “neuron projection extension”, or “dendrite development” (fig. S6B), the cluster associated with inhibitory neurons was enriched for “GABA synthesis, release, reuptake and degradation”, “GABA receptor

signaling", or "GABA synapse" (fig. S6C), both corroborating meaningful peak-to-gene links in each of the clusters.

To identify putative regulatory elements that underlie the transcriptomic differences between ExN L2-3 IT and ExN L3-5 IT, we calculated differential accessibility and overrepresented motifs (Materials and Methods) between these neuronal populations throughout midfetal and late fetal development. Using this strategy, we have identified the MEIS2 motif MA0774.1 as one of the overrepresented motifs in the ExN L2-3 IT subclass (Materials and Methods, table S6). Furthermore, we calculated motif activity scores using chromVAR (*25*) and found that ExN L2-3 IT has both a higher *MEIS2* gene expression and a higher motif activity score when compared to ExN L3-5 IT (Fig. 3D). Because MEIS2 is a transcription factor enriched in upper layer neurons in primates (*16, 23*) and due to its relevance for neuropsychiatric disorders (*26*), we calculated MEIS2 transcription factor footprints across the whole genome. This strategy allowed us to further explore the enrichment of active MEIS2 transcription factor binding sites (TFBS) between these two cell subclasses throughout the analyzed developmental periods (Materials and Methods). We found that ExN L2-3 IT had the highest footprint enrichment during midfetal development (PCD 104-112), whereas ExN L3-5 IT had the lowest footprint enrichment during late fetal development (PCD 155), indicating the selective involvement of MEIS2 in the regulation of target genes in ExN L2-3 IT (Fig. 3E). Indeed, quantitative immunofluorescence showed that there were significantly fewer MEIS2-expressing cells in L3-5 compared to L2-3 of dlPFC at PCD155 (Fig. 3F). To gain insights into the biological processes regulated by the potential targets of MEIS2, we first identified the genes closest to the MEIS2 motif binding sites (Materials and Methods, table S6) and assigned a score for each gene based on the average expression of these target genes in ExN L2-3 IT and ExN L3-5 IT (Materials and Methods). We then performed a functional enrichment analysis and found that, overall, MEIS2-regulated genes in ExN L2-3 IT and ExN L3-5 IT were highly conserved for most biological processes. However, we observed a specific enrichment for synapse-associated terms, such as "trans-synaptic signaling" and "synapse organization" in ExN L3-5 IT, and "cell morphogenesis" in ExNL2-3 IT (table S6, fig. S6D and 6E). These differences can be

explained by the differences in maturation time across these two populations, as ExN L3-5 IT are generated and start maturing earlier than ExN L2-3 IT.

One of the genes potentially regulated by MEIS2 in IT excitatory neurons is the *Nuclear factor I/A* (*NFIA*), a gene known to be regulated by MEIS2 in retinal progenitor cells (*27*). *NFIA* has been linked to callosal hypoplasia, which likely reflects malformations of upper-layer excitatory neurons, and language delay, which was an enriched term for ExN L2-3 IT (fig. S6D and 6E) (*28*). By analyzing the distribution of accessible chromatin peaks in the vicinity of *NFIA* across the two neuronal subclasses and developmental periods, we identified 8 active MEIS2 binding sites within 200kb upstream from the *NFIA* transcription start site (Fig. 3G). We also found three peak-to-gene links (i.e., peaks that show higher co-activity with *NFIA* gene expression; Materials and Methods) with one of the links containing an active MEIS2 binding site (chr1-163553896-163555161) ~181kb upstream of *NFIA* transcription starting site, indicating that it could be a potential enhancer for *NFIA*.

Patch-seq of midfetal and late fetal macaque dlPFC cells identified transcriptomic signature defining electrophysiological maturation

The midfetal and late fetal periods are critical stages in cortical development, marked by notable alterations in neuronal morphology, physiology, and gene expression (*29*). To evaluate the morphology of cortical neurons, dlPFC slices from mid-fetal PCD100 and late-fetal PCD155 macaques were infected with lentivirus (LV) expressing a fluorescent protein (mScarlet) (fig. S7A) that infects mostly (>90%) neurons (*30*). The analyzed neurons displayed a relatively immature morphology, characterized by a limited number of neurites. As expected, PCD155 neurons exhibited significantly greater complexity (fig. S7, B-C), with longer total dendritic length (fig. S7D), increased branching points (fig. S7E), and more endings (fig. S7F), compared to neurons in PCD100 brains. Thus, neurons in the primate PFC undergo substantial morphological maturation from midfetal to late fetal development.

To gain a comprehensive understanding of the molecular mechanisms that drive neuronal maturation in midfetal PFC, we employed Patch-seq, which allows for electrophysiological and gene expression analyses of the same cell (*31*). We analyzed dlPFCs collected from 14 individual rhesus macaque at 10 fetal ages from PCD87 to PCD155 (table S1), thereby facilitating the dissection of neuronal maturation processes with high reliability (Fig. 4A, fig. S7G-H, and table S7). In total, we collected high-quality electrophysiology and RNA-seq data from 210 cells (table S7). Given the inherent immaturity of midfetal neurons, it is difficult to accurately identify neurons based solely on cell morphology or electrophysiological properties. Therefore, we performed cell annotation before any downstream analysis to minimize the risk of including non-neuronal cells in our analysis. We used our snRNA-seq data (Fig. 2) as a reference dataset to infer Patch-seq cell types by mapping Patch-seq cells onto the reference UMAP (Fig. 4B, table S7). To ascertain the precision of cell annotation outcomes, we assessed the expression of relevant markers in each assigned cell type and confirmed that the enriched expression of correspondent markers was consistent with the annotated cell types (fig. S7I). As expected, both excitatory neurons (ExNs) and interneurons (InNs) generated evoked action potentials (APs), whereas the remaining cell types (Astro, Endo, MG, Oligo, VLMC) failed to exhibit evoked APs, except for OPCs, which were previously shown to produce evoked APs (fig. S7J, table S7) (*32*). These data provided further evidence supporting the reliability of our cell annotation (Fig. 4B, table S7). Approximately 70% of the total 210 cells were identified as neurons, comprising 100 ExNs and 50 InNs (table S7). Out of the 100 ExNs, 88 were classified as IT neurons (table S7). In order to evaluate the similarity among the IT neurons, we investigated the electrophysiological characteristics of three major IT subtypes (L2-3, L2-3/L3-5, and L3-5) across different ages. Our findings revealed that these IT neurons exhibited comparable electrophysiological features (fig. S8, A-D). Based on these outcomes, we decided to combine all IT neuron types for our downstream analysis.

We employed a pseudotime trajectory analysis to infer a maturation trajectory by integrating 232 differentially expressed genes across age groups in all identified IT neurons (*33*) (Fig. 4C, table S8). Our

analysis revealed a trajectory characterized by the progressive maturation of IT neurons from younger (PCD87) to older (PCD155) ages (Fig. 4C, fig. S8). To investigate the electrophysiological maturation of these neurons, we divided neurons recorded from 14 macaques into four age groups (PCD87-96, PCD99-104, PCD106-112, and PCD155). The electrophysiological properties of neurons can provide critical insights into their level of maturity, as evidenced by their capacity to exhibit evoked APs. Indeed, we observed that the proportion of IT neurons exhibiting APs increased from 3.1% in the PCD87-96 group to 8.3% in the PCD99-104 group, and 33.3% in the PCD106-112 group. Notably, all neurons analyzed at PCD155 demonstrated evoked APs, providing strong evidence for electrophysiological maturation (fig. S8F, table S7). Given that various electrophysiological features offer unique perspectives on maturation, we opted to explore maturation through the lens of the following electrophysiological features: membrane capacitance (C_m), input resistance (R_{in}), resting membrane potential (RMP), and inward sodium current (I_{Na}). Our findings revealed an increase in the C_m from PCD87-96 and PCD99-104 to PCD106-112 and PCD155 (Fig. 4E). This increase was not linear, as we did not observe any changes between PCD87-96 and PCD99-104, nor from PCD106-112 to PCD155 (Fig. 4E). Regardless, the increase in C_m reflects the enlargement of the cell body and more complex cellular structures during the maturation of neurons. In contrast, there was a gradual decline on the averaged value of R_{in} observed from PCD87-91 to PCD155 (Fig. 4F). This effect may be attributed to an increase in the number of ion channels in the neuronal membrane, which facilitates rapid and efficient movement of ions across the membrane. Moreover, the morphological changes that occur in dendrites (fig. S7B-F) and spines during maturation may contribute to alterations in signal processing and integration, further enhancing neuronal function. We also observed a conspicuous pattern of increasingly negative (more polarized) RMP from PCD87-91 to PCD155 (Fig. 4G). This observation serves as evidence of a developmental progression in the ion channels and pumps of these neurons. This maturation of ion channels and pumps leads to a more negative RMP in neurons, allowing for improved electrical signal processing and transmission. During neuronal development, the current density of I_{Na} amplifies (values become more negative, with the negative sign as an indication of the direction of current), thereby increasing the neurons' capacity to generate action potentials. Our results

indicate a significant increase in the amplitude of the I_{Na} from PCD106-112 to PCD155, with a small increase already evident from PCD99-104 to PCD106-112 (Fig. 4H). This suggests that IT neurons in the dlPFC acquire the ability to initiate and transmit APs after PCD112. In summary, our analyses showed a progression in maturation across all four electrophysiological properties. However, it is noteworthy that the temporal dynamics of the four electrophysiological properties were not identical. While R_{in} and RMP exhibited a progressive decrease across all four age groups, I_{Na} displayed a marked decline only at PCD155. Conversely, C_m exhibited a significant increase at PCD106-112 (Fig. 4, E-H). Our study has uncovered distinct profiles in the temporal dynamics of electrophysiological maturation, where each property exhibits a different speed of maturation.

In the adult cortex, different neuronal types exhibit distinct electrophysiological properties (*34*). We therefore investigated whether different types of neurons in the fetal macaque brain also display distinct electrophysiological features. Out of the 210 patch-seq cells we analyzed, 50 were identified as InNs. Similar to IT ExNs (fig. S9), InNs exhibited a progressively negative RMP and a sharp change in the I_{Na} from PCD106-112 to PCD155. The overall trends for C_m and RMP were similar in both IT ExNs and InNs, but two differences were observed. Specifically, for C_m, the differences between PCD106-112 and PCD155 were more pronounced in InNs (fig. S9A), whereas for RMP, the differences between PCD87-96 and PCD99-104 were less pronounced in InNs (fig. S9B), compared to those in ExNs. Therefore, both InNs and IT ExNs exhibited similar trends in maturation across all electrophysiological features in the prefrontal cortex of fetal brains.

Ultimately, the maturation of neurons is driven by changes in gene expression profiles. We postulated that the divergent trends of the four electrophysiological features observed across the maturation stages may be attributable to the expression of different genes. In order to discern the genes that are correlated with individual electrophysiological features, we conducted a correlation analysis between the specific electrophysiological data of all IT neurons and the expression levels of each gene across all IT neurons. Applying an r value cutoff of 0.5 ($r > 0.5$ or $r < -0.5$), we identified 39 genes, 9 genes, 81 genes,

and 139 genes that are associated with the electrophysiological features of C_m, R_{in}, RMP, and I_{Na}, respectively (fig. S10A, table S9). On the other hand, genes that are not expected to exhibit correlation with electrophysiological features, including *GAPDH* and *TBP* (fig. S10B), showed no significant correlation with any of the electrophysiological features.

Several genes, including *CAMK2A* and *MICAL2*, exhibited high correlation with all four investigated electrophysiological features (Fig. 4, E-H). However, the correlation values differed across each electrophysiological feature (table S9). This finding suggests that while certain genes may exhibit a preferential correlation with one of the electrophysiological features, they may also demonstrate a significant, but less pronounced, correlation with other electrophysiological features that align with the principal trend of neuronal maturation (fig. S10A, table S9). We selected genes that exhibited significant correlation with each of the four electrophysiological features and plotted their expression profiles across four age cohorts (PCD87-96, PCD99-104, PCD106-112, and PCD155). This uncovered notable variations in the expression levels of most of the top-ranked genes across the different age groups, indicative of their involvement in the maturation of neurons (Fig. 4, E-H). To validate our Patch-seq data, we performed in situ hybridization on dlPFC sections of PCD100 and PCD155 macaques for select genes that demonstrated significant correlation with each of the four electrophysiological features: *CAMK2A*, *MICAL2*, *NRGN*, *RAPGEF4*, and *VXN*. Consistent with the Patch-seq results, the RNA expression levels of all five tested genes were higher in PCD155 compared to those in PCD100 brain tissue (Fig. 4D, fig. S10D-E).

Gene Ontology (GO) analysis (fig. S11, A-C) on the genes associated with electrophysiological features showed that the gene set associated with C_m included “regulation of neuronal synaptic plasticity”, “regulation of monoatomic ion transport”, and “regulation of plasma membrane bounded cell projection organization”. In contrast, the genes associated with RMP were enriched with “ephrin receptor signaling pathway”, “regulation of GTPase activity”, “synaptic signaling”, and “regulation of vesicle-mediated transport”. Additionally, the I_{Na}-correlated genes were enriched for “synapse organization”, “regulation of

neuron projection development", and "actin filament-based process". Therefore, the developmental maturation of different electrophysiological features may be driven by differential sets of genes.

In summary, our analyses of prefrontal cortical neurons from 14 rhesus macaque across midfetal and late-fetal development revealed evidence of neuronal maturation across three distinct aspects: morphological, transcriptomic, and electrophysiological properties. Moreover, we observed distinct temporal dynamics in electrophysiological maturation, during which each property exhibits a unique rate of maturation. Also, we identified critical genes associated with primate neuronal maturation by utilizing both transcriptomic and electrophysiological approaches.

RAPGEF4 is crucial for the morphological and electrophysiological maturation of excitatory neurons

Our Patch-seq analysis demonstrated a marked upregulation of *RAPGEF4* expression in IT neurons during cortical development (Fig. 4D, 4H), which was also corroborated by our snRNA-seq data (Fig. 5A). RAPGEF4 (Rap Guanine Nucleotide Exchange Factor 4), also known as EPAC2 (exchange protein directly activated by cyclic AMP 2), is a regulator of small GTPase signaling and a protein kinase A (PKA)-independent cAMP target (*35, 36*). We found that *RAPGEF4* exhibited a high degree of correlation with various electrophysiological features, with the highest correlation observed with I_{Na} (r = -0.72). The second highest correlation was observed with RMP (r = -0.52), while slightly lower correlations were observed with C_m (r = 0.45) and R_{in} (r = -0.39) (fig. S12A).

To investigate whether *RAPGEF4* is important for neuronal maturation, we infected ex vivo macaque brain slices with LV expressing mScarlet and shRNA against *RAPGEF4* (sh*RAPGEF4*) together with LV expressing mNeonGreen and control shRNA (sh*NC*) (fig. S12B) and performed morphological and electrophysiological analyses of targeted neurons (Fig. 5B). The neurons with *RAPGEF4* knockdown (sh*RAPGEF4*, mScarlet+) exhibited reduced dendritic complexity (Fig. S5C-E), total dendritic length (Fig. 5F), branching points (Fig. 5G) and number of endings (Fig. 5H), compared to neurons infected with sh*NC*

(mNeonGreen+mScarlet-). In addition, *RAPGEF4* knockdown neurons (sh*RAPGEF4*) exhibited smaller I_{Na} (Fig. 5I-J) and less negative RMP (Fig. 5K), without significant changes in C_m and R_{in}, compared to control neurons (Fig. 5L-M, and table S10). These results indicate that a deficiency of *RAPGEF4* in neurons leads to abnormal maturation of I_{Na} and RMP, which is consistent with our finding that *RAPGEF4* had a strong correlation with I_{Na} (r = -0.72) and RMP (r = -0.52), but not with C_m (r = 0.45) and R_{in} (r = -0.39) (Fig. 4G-H, fig. S12A).

RAPGEF4 is a guanine exchange factor enriched in neurons compared to other cell types (*36*). The levels of *RAPGEF4* increase in the human brain from fetal development to adulthood, specifically in the cortex, compared to other tissues or organs (fig. S12C) (*37*). Based on our observations in macaque, we hypothesized that the correlation between *RAPGEF4* and electrophysiological properties also occurs in humans. We subsequently infected human midfetal cortical brain slices with LV expressing sh*RAPGEF4* and performed patch-clamp recording. We also observed reduced I_{Na} and RMP, but not C_m and R_{in}, in human neurons with *RAPGEF4* knockdown compared to controls (fig. S12D-I, table S10). The role of RAPGEF4 in regulation of RMP in both macaque and human neurons is consistent with the fact that genes driving RMP maturation are enriched for "regulation of GTPase activity" (fig. S11A).

Therefore, these data validate our approach to identify genes that drive the maturation of specific electrophysiological features and reveal the novel role of *RAPGEF4* in morphological and electrophysiological maturation of IT neurons in both macaque and human cortical development.

CHD8 **knockdown leads to impaired maturation of human cortical excitatory neurons**

Recent advances in genomics have revealed important roles of chromatin regulators during midfetal PFC development and their implication in neurodevelopmental disorders (*38, 39*). CHD8 (Chromodomain Helicase DNA-binding protein 8) is a chromatin remodeling protein that plays a crucial role in gene expression regulation during brain development and has been linked to ASD (*39-43*). To investigate the

role of *CHD8* during human midfetal dlPFC development, a critical developmental period for ASD (*44, 45*), we knocked down *CHD8* expression in ex vivo human fetal brain slices using LV expressing sh*CHD8* and mScarlet (red) (Fig. 6A, fig. S13A), together with LV expressing *shNC* and mNeonGreen (green). Neurons with *CHD8* knockdown displayed significantly shorter dendrites compared to control neurons (Fig. 6B-E, fig. S13B-D), suggesting that a deficiency in CHD8 disrupts morphological maturation of cortical neurons during midfetal development, which is consistent with previous findings in mice (*41*).

We performed Patch-seq on 87 cells from slices that contained both *CHD8* knockdown and control cells (Fig. 6A, fig. 13E-F). To determine the cellular identity of each recorded cell, we compared its transcriptome with the snRNA-seq data we generated (Fig. 2) and assigned each queried cell a specific cell type and mapped them onto the snRNA-seq UMAP reference (Fig. 6C, table S11). To verify the accuracy of our cell type annotations, we plotted the gene expression of the corresponding marker genes for each major cell type and observed elevated expression levels of cell marker genes in appropriate cell types (fig. S13G). Of the 87 cells analyzed, 71% were identified as neurons, consisting of 50 ExNs and 12 InNs. Among the ExNs, 45 cells were classified as IT neurons, which were subsequently selected for further analysis (Fig. 6C, table S11). The 45 IT neurons were further stratified into two groups: the sh*NC* group (24 neurons) and the sh*CHD8* group (21 neurons) (table S11). The levels of *CHD8* were significantly reduced in the sh*CHD8* group compared to shNC group (Fig. 6F).

The excitatory IT neurons with *CHD8* knockdown had a significant decrease in both R_{in} and RMP (Fig. 6I and J) but not in C_m and I_{Na} (Fig. 6H and K, fig. S13H), compared to the controls. Therefore, *CHD8* knockdown produces a discernible impact on the electrophysiological properties of midfetal human neurons, which is consistent with its role during early development (*41, 42*). Since each electrophysiological property follows distinctive temporal dynamics of maturation (Fig. 4), the differential impact of CHD8 and RAPGEF4 knockdown reflects distinct roles of these two proteins in neuronal maturation during primate fetal development.

Conclusions

In this study, we have generated and analyzed a multimodal dataset, which included snRNA-seq, snATAC-seq, and Patch-seq of the rhesus macaque dlPFC during midfetal and late fetal development. We identified differences across cell types in their maturation trajectories as well as critical developmental periods for the maturation of specific electrophysiological properties in excitatory and inhibitory neurons.

We confirmed that excitatory neurons gain their laminar and projection identities earlier than interneuronal final specification, even though their electrophysiological maturation occurs at a similar pace. This corroborates previous findings that pointed to the relevance of extrinsic factors to the final specification of interneurons during perinatal development (*13, 46*). We focused our analyses on the intratelencephalic-projecting excitatory neurons due to their relevance both to primate brain evolution and their association to neuropsychiatric disorders. We uncovered several differences both at gene expression and accessible chromatin levels. Our integrative analysis highlighted MEIS2 as a key transcriptional factor relevant for L2-3 IT, but not other IT, neuronal development.

By integrating electrophysiology, morphology, and functional genomics analyses of primate dlPFC development, we were able to find that different electrophysiological properties mature at different rates. Although most of the genes involved in neuronal maturation were associated with all the analyzed electrophysiological properties, we also uncovered several genes that are associated with specific electrophysiological features. This led us to functionally evaluate the role of one of those genes: *RAPGEF4*. By knocking down the expression of *RAPGEF4* in organotypic slices of macaque dlPFC, we confirmed that *RAPGEF4* is important for the developmental maturation of resting membrane potential and inward sodium currents. RAPGEF4 is a Rap small GTPase guanine exchange factor and is a direct target of cAMP, independent of canonical cAMP-dependent PKA signaling. RAPGEF4 has been shown to regulate dendritic spine remodeling in mice and its deficiency in mice leads to synaptic plasticity and learning and memory deficits (*47, 48*). The role of RAPGEF4 in primate brain development or human disease is unknown. Dysregulation of the cAMP pathway has been implicated in a wide range of neurological disorders,

including fragile X syndrome. Fragile X syndrome is an ASD known to have reduced cAMP signaling and a potential treatment to elevate cAMP levels through phosphodiesterase inhibition is currently in clinical trial (*49-51*). The direct involvement of RAPGEF4 in fragile X syndrome or ASD is unknown. Our study demonstrates that RAPGEF4 may be one of the small GTPase regulators driving neuronal maturation during primate brain development, especially for RMP an electrophysiological feature regulated by GTPase signaling.

Finally, to demonstrate the potential of our experimental platform in exploring the developmental origin of human diseases, we have knocked down the expression of a high-confidence ASD gene – *CHD8* – in human organotypic slices and showed that proper maturation of excitatory neurons was affected. These neurons were more immature both morphologically and electrophysiologically. Together, our results demonstrate the usefulness of our approach and show that it will serve as the basis for future studies aiming at understanding how genes, and the mechanisms that regulate their expression, can affect the physiological maturation of different neurons, including those implicated in brain disorders.

References

1. T. M. Preuss, S. P. Wise, Evolution of prefrontal cortex. *Neuropsychopharmacology* **47**, 3-19 (2022).
2. J. B. Smaers, A. Gomez-Robles, A. N. Parks, C. C. Sherwood, Exceptional Evolutionary Expansion of Prefrontal Cortex in Great Apes and Humans. *Curr Biol* **27**, 714-720 (2017).
3. A. M. M. Sousa, K. A. Meyer, G. Santpere, F. O. Gulden, N. Sestan, Evolution of the Human Nervous System Function, Structure, and Development. *Cell* **170**, 226-247 (2017).
4. R. Levy, P. S. Goldman-Rakic, Association of storage and processing functions in the dorsolateral prefrontal cortex of the nonhuman primate. *J Neurosci* **19**, 5149-5158 (1999).
5. M. F. Kritzer, P. S. Goldman-Rakic, Intrinsic circuit organization of the major layers and sublayers of the dorsolateral prefrontal cortex in the rhesus monkey. *J Comp Neurol* **359**, 131-143 (1995).
6. D. A. Lewis, K. Mirnics, Transcriptome alterations in schizophrenia: disturbing the functional architecture of the dorsolateral prefrontal cortex. *Prog Brain Res* **158**, 141-152 (2006).

7. R. Cools, A. F. T. Arnsten, Neuromodulation of prefrontal cortex cognitive function in primates: the powerful roles of monoamines and acetylcholine. *Neuropsychopharmacology* **47**, 309-328 (2022).
8. K. Pattabiraman, S. K. Muchnik, N. Sestan, The evolution of the human brain and disease susceptibility. *Curr Opin Genet Dev* **65**, 91-97 (2020).
9. M. T. Schmitz *et al.*, The development and evolution of inhibitory neurons in primate cerebrum. *Nature* **603**, 871-877 (2022).
10. T. J. Nowakowski *et al.*, Spatiotemporal gene expression trajectories reveal developmental hierarchies of the human cortex. *Science* **358**, 1318-1323 (2017).
11. A. Bhaduri *et al.*, An atlas of cortical arealization identifies dynamic molecular signatures. *Nature* **598**, 200-204 (2021).
12. M. B. Johnson, C. A. Walsh, Cerebral cortical neuron diversity and development at single-cell resolution. *Curr Opin Neurobiol* **42**, 9-16 (2017).
13. L. Lim, D. Mi, A. Llorca, O. Marin, Development and Functional Diversification of Cortical Interneurons. *Neuron* **100**, 294-313 (2018).
14. R. C. Bandler, C. Mayer, G. Fishell, Cortical interneuron specification: the juncture of genes, time and geometry. *Curr Opin Neurobiol* **42**, 17-24 (2017).
15. B. J. Molyneaux, P. Arlotta, J. R. Menezes, J. D. Macklis, Neuronal subtype specification in the cerebral cortex. *Nat Rev Neurosci* **8**, 427-437 (2007).
16. S. Ma *et al.*, Molecular and cellular evolution of the primate dorsolateral prefrontal cortex. *Science* **377**, eabo7257 (2022).
17. J. Berg *et al.*, Human neocortical expansion involves glutamatergic neuron diversification. *Nature* **598**, 151-158 (2021).
18. F. M. Krienen *et al.*, Innovations present in the primate interneuron repertoire. *Nature* **586**, 262-269 (2020).
19. L. Beaulieu-Laroche *et al.*, Allometric rules for mammalian cortical layer 5 neuron biophysics. *Nature* **600**, 274-278 (2021).
20. N. Micali *et al.*, Molecular programs of regional specification and neural stem cell fate progression in developing macaque telencephalon. *bioRxiv*, 2022.2010.2018.512724 (2022).
21. B. G. Rash *et al.*, Gliogenesis in the outer subventricular zone promotes enlargement and gyrification of the primate cerebrum. *Proc Natl Acad Sci U S A* **116**, 7089-7094 (2019).
22. V. Luria, S. Ma, M. Shibata, K. Pattabiraman, N. Sestan, Molecular and cellular mechanisms of human cortical connectivity. *Curr Opin Neurobiol* **80**, 102699 (2023).

23. M. Shibata *et al.*, Regulation of prefrontal patterning and connectivity by retinoic acid. *Nature* **598**, 483-488 (2021).

24. M. Li *et al.*, Integrative functional genomic analysis of human brain development and neuropsychiatric risks. *Science* **362**, (2018).

25. A. N. Schep, B. Wu, J. D. Buenrostro, W. J. Greenleaf, chromVAR: inferring transcription-factor-associated accessibility from single-cell epigenomic data. *Nat Methods* **14**, 975-978 (2017).

26. F. Erdogan *et al.*, Characterization of a 5.3 Mb deletion in 15q14 by comparative genomic hybridization using a whole genome "tiling path" BAC array in a girl with heart defect, cleft palate, and developmental delay. *Am J Med Genet A* **143A**, 172-178 (2007).

27. N. Dupacova, B. Antosova, J. Paces, Z. Kozmik, Meis homeobox genes control progenitor competence in the retina. *Proc Natl Acad Sci U S A* **118**, (2021).

28. Y. Negishi *et al.*, Truncating mutation in NFIA causes brain malformation and urinary tract defects. *Hum Genome Var* **2**, 15007 (2015).

29. J. C. Silbereis, S. Pochareddy, Y. Zhu, M. Li, N. Sestan, The Cellular and Molecular Landscapes of the Developing Human Central Nervous System. *Neuron* **89**, 248-268 (2016).

30. Y. Guo *et al.*, Elevated levels of FMRP-target MAP1B impair neuronal development and social behaviors via autophagy pathway. *Nature Communications* **in press** (2023).

31. C. R. Cadwell *et al.*, Electrophysiological, transcriptomic and morphologic profiling of single neurons using Patch-seq. *Nat Biotechnol* **34**, 199-203 (2016).

32. R. Karadottir, N. B. Hamilton, Y. Bakiri, D. Attwell, Spiking and nonspiking classes of oligodendrocyte precursor glia in CNS white matter. *Nat Neurosci* **11**, 450-456 (2008).

33. X. Qiu *et al.*, Reversed graph embedding resolves complex single-cell trajectories. *Nat Methods* **14**, 979-982 (2017).

34. X. Jiang *et al.*, Principles of connectivity among morphologically defined cell types in adult neocortex. *Science* **350**, aac9462 (2015).

35. J. L. Bos, Epac: a new cAMP target and new avenues in cAMP research. *Nat Rev Mol Cell Biol* **4**, 733-738 (2003).

36. J. de Rooij *et al.*, Epac is a Rap1 guanine-nucleotide-exchange factor directly activated by cyclic AMP. *Nature* **396**, 474-477 (1998).

37. G. T. Consortium, Human genomics. The Genotype-Tissue Expression (GTEx) pilot analysis: multitissue gene regulation in humans. *Science* **348**, 648-660 (2015).

38. F. K. Satterstrom *et al.*, Large-Scale Exome Sequencing Study Implicates Both Developmental and Functional Changes in the Neurobiology of Autism. *Cell* **180**, 568-584 e523 (2020).

39. Y. Katayama *et al.*, CHD8 haploinsufficiency results in autistic-like phenotypes in mice. *Nature* **537**, 675-679 (2016).
40. R. Bernier *et al.*, Disruptive CHD8 mutations define a subtype of autism early in development. *Cell* **158**, 263-276 (2014).
41. O. Durak *et al.*, Chd8 mediates cortical neurogenesis via transcriptional regulation of cell cycle and Wnt signaling. *Nat Neurosci* **19**, 1477-1488 (2016).
42. J. Cotney *et al.*, The autism-associated chromatin modifier CHD8 regulates other autism risk genes during human neurodevelopment. *Nat Commun* **6**, 6404 (2015).
43. A. Sugathan *et al.*, CHD8 regulates neurodevelopmental pathways associated with autism spectrum disorder in neural progenitors. *Proc Natl Acad Sci U S A* **111**, E4468-4477 (2014).
44. N. N. Parikshak *et al.*, Integrative functional genomic analyses implicate specific molecular pathways and circuits in autism. *Cell* **155**, 1008-1021 (2013).
45. A. J. Willsey *et al.*, Coexpression networks implicate human midfetal deep cortical projection neurons in the pathogenesis of autism. *Cell* **155**, 997-1007 (2013).
46. A. Kepecs, G. Fishell, Interneuron cell types are fit to function. *Nature* **505**, 318-326 (2014).
47. K. M. Woolfrey *et al.*, Epac2 induces synapse remodeling and depression and its disease-associated forms alter spines. *Nat Neurosci* **12**, 1275-1284 (2009).
48. K. A. Jones, M. Sumiya, K. M. Woolfrey, D. P. Srivastava, P. Penzes, Loss of EPAC2 alters dendritic spine morphology and inhibitory synapse density. *Molecular and cellular neurosciences* **98**, 19-31 (2019).
49. E. Berry-Kravis, M. Hicar, R. Ciurlionis, Reduced cyclic AMP production in fragile X syndrome: cytogenetic and molecular correlations. *Pediatr Res* **38**, 638-643 (1995).
50. D. J. Kelley *et al.*, The cyclic AMP cascade is altered in the fragile X nervous system. *PLoS One* **2**, e931 (2007).
51. E. M. Berry-Kravis *et al.*, Inhibition of phosphodiesterase-4D in adults with fragile X syndrome: a randomized, placebo-controlled, phase 2 clinical trial. *Nat Med* **27**, 862-870 (2021).

Acknowledgements: We thank Y. Xing, S. Krebsbach, D. Phan, M. Weidenfeller, and H. Thurston for technical assistance; K. Knobel at the Waisman IDD Model Core for core services; Dr. Heather Simmons, Director of Pathology Services, WNPRC, for non-human primate tissue acquisition.

Funding: This work was supported by the following: National Institutes of Health grant R01MH118827(to X.Z); National Institutes of Health grant R01NS105200 (to X.Z); National Institutes of Health grant R01HD064743 (to Q.C), National Institutes of Health R01NS064025 (to D.W), National Institutes of Health R01AG067025 (to D.W), National Institutes of Health RF1MH128695 (to D.W), National Institutes of Health P51 OD011106 (to the WNPRC), National Institutes of Health P50HD105353 (to the Waisman Center), National Institutes of Health R24HD000836 (to the Birth Defects Research Laboratory), DOD IIRA grant (to X.Z.), Jenni and Kyle Professorship (to X.Z.), NARSAD Young Investigator Grant from the Brain and Behavior Research Foundation 28721 (to A.M.M.S.), Wisconsin National Primate Research Center Pilot Research Award (to A.M.M.S.), and Simons SFARI pilot grant (to X.Z., A.M.M.S., Q.C., and D.W).

Competing interests: The authors declare that they have no competing interests.

Authors contributions: Y.G., Q.D., Q.C., X.Z., and A.M.M.S. conceived and designed the study. Y.G., Q.D., R.D.R., M.S., D.K.S., and A.M.M.S. performed the experiments. K.H.A., J.S., T.J., S.L., and D.W. analyzed the genomics data. J.E.L., D.D., and I.G. provided the analyzed specimens. Y.G., Q.D., K.H.A., Q.C., X.Z., and A.M.M.S. wrote the manuscript. All authors edited the manuscript.

Data and materials availability:

The data can be interactively visualized at https://daifengwanglab.shinyapps.io/DevMacaquePFC/. All other data are available in the main paper or supplementary information.

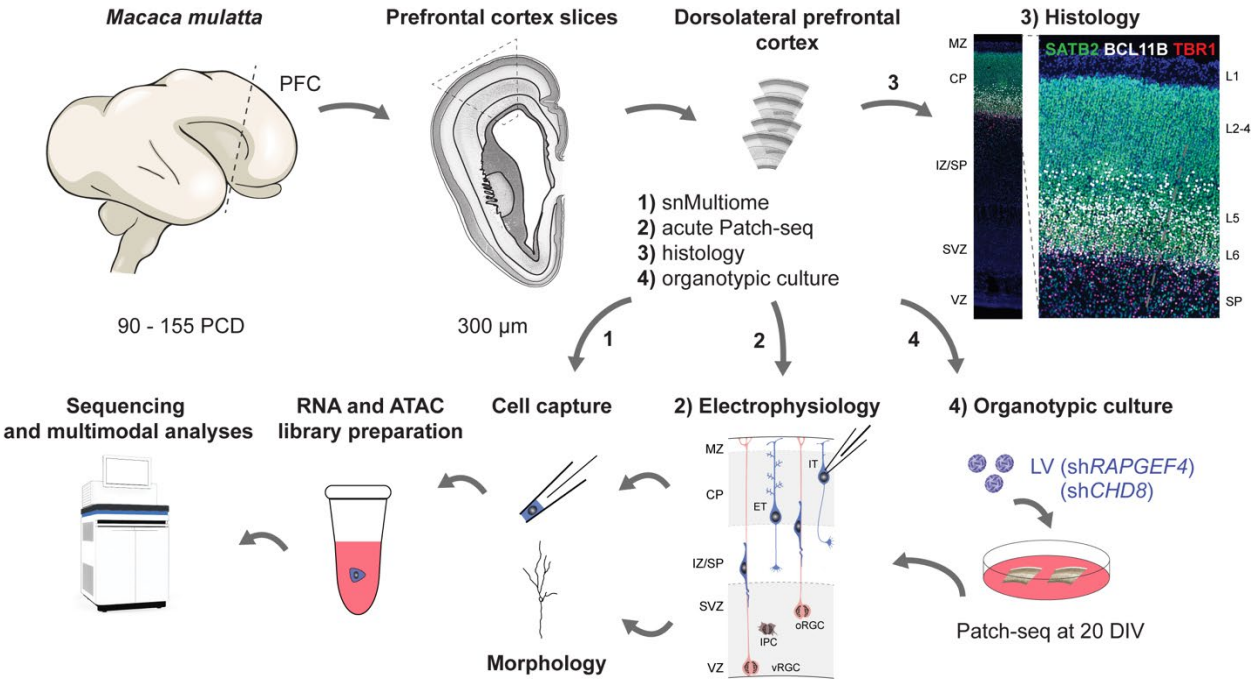

Fig. 1. Schematic of the study design

The frontal cortex of Rhesus macaque (*Macaca mulatta*) brains, aged from postconceptional day (PCD) 87 to 155, were dissected and sectioned at 300 µm. Acute dorsolateral prefrontal cortices were analyzed using Patch-seq and single-nucleus multiome (snRNA-seq and snATAC-seq). Tissue from the same specimens, as well as human midfetal tissue, was also used to culture organotypic slices for functional analyses of select genes (*RAPGEF4* and *CHD8*). Validation of key findings was also performed by multiplexed immunostaining and single-molecule fluorescent in situ hybridization on dlPFC sections from the contralateral hemisphere of the same specimens (table S1). Finally, we have performed an integrative analysis of the generated multimodal dataset.

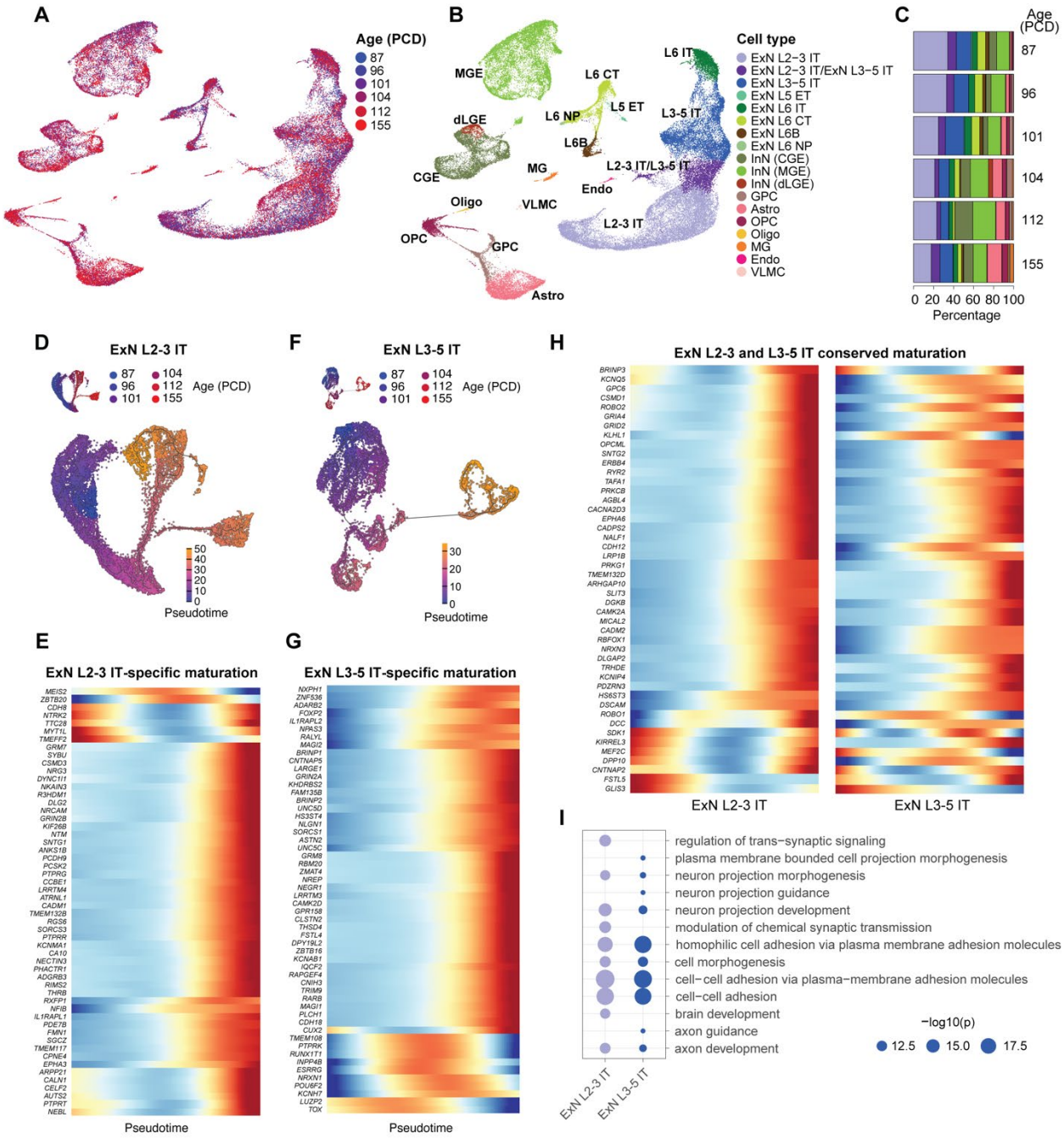

Fig. 2. Single-nucleus transcriptomic atlas of rhesus macaque dlPFC cells across midfetal and late fetal development

(A-B) UMAP visualization of all the cell classes and subclasses. Cells are colored according to **(A)** age in postconceptional days (PCD) or to **(B)** cell subclass. **(C)** Bar plot showing the cell composition of the dlPFC

throughout midfetal and late fetal development. **(D)** UMAP visualization of the maturation trajectory of ExN L2-3 IT cells; top panel is colored according to postconceptional days, whereas bottom panel is colored according to inferred pseudotime. **(E)** Gene expression variation with pseudotime of 50 genes specific to ExN L2-3 IT. **(F)** UMAP visualization of the maturation trajectory of ExN L3-5 IT cells; top panel is colored according to postconceptional days, whereas bottom panel is colored according to inferred pseudotime. **(G)** Gene expression variation with pseudotime of 50 genes specific to ExN L3-5 IT. **(H)** Gene expression variation with pseudotime for the genes with conserved expression in ExN L2-3 IT and ExN L3-5 IT maturation. ExN, excitatory neurons; IT, intratelencephalic; ET, extratelencephalic; CT, corticothalamic; NP, near-projecting; InN, inhibitory neurons; CGE, caudal ganglionic eminence; MGE, medial ganglionic eminence; dLGE, dorsal lateral ganglionic eminence; GPC, glial precursor cells; Astro, astrocytes; OPC, oligodendrocyte precursor cells; Oligo, oligodendrocytes; MG, microglia; Endo, endothelial cells; VLMC, vascular leptomeningeal cells.

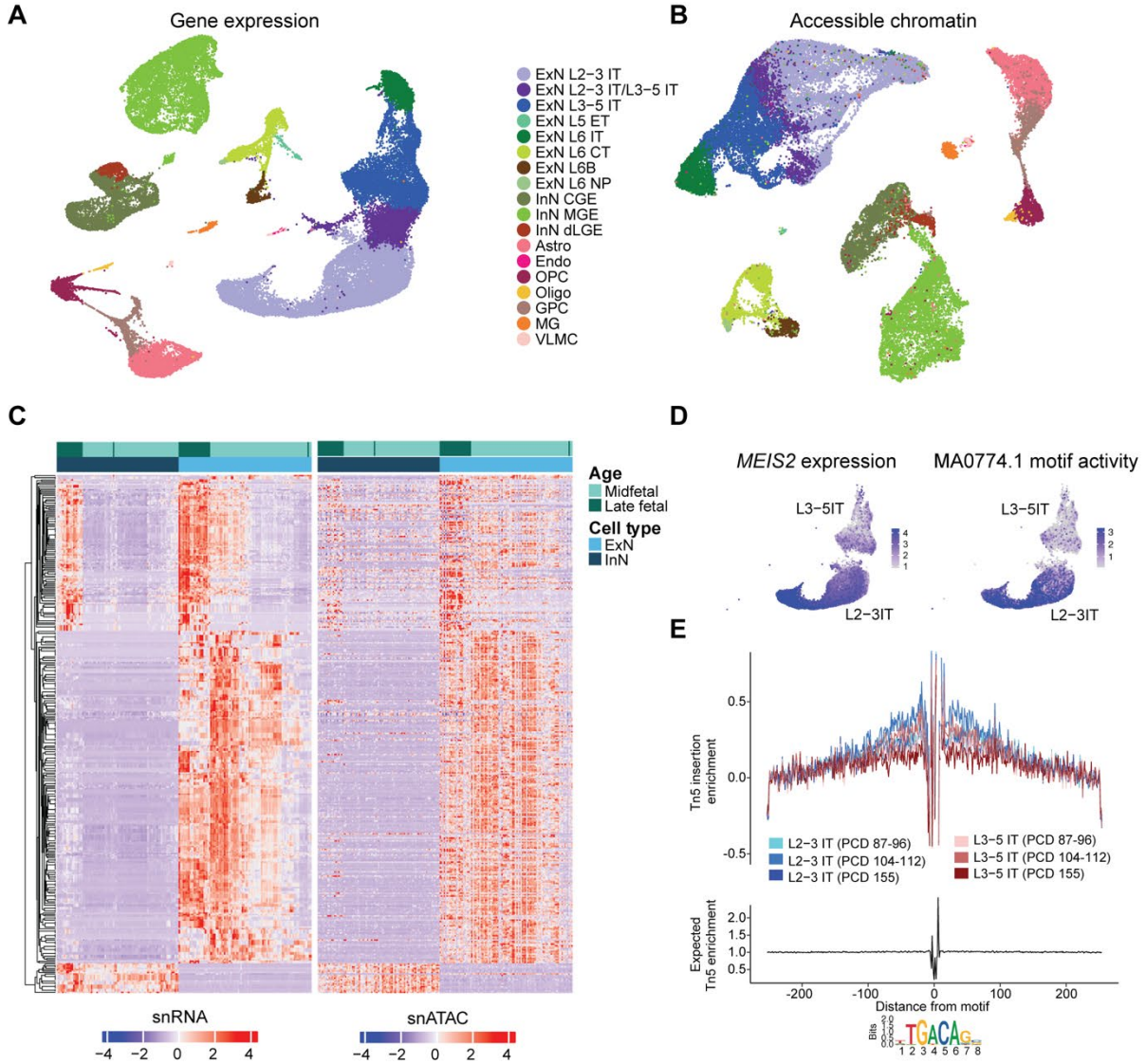
A
Gene expression
ExN L2−3 IT
ExN L2−3 IT/L3−5 IT
ExN L3−5 IT
ExN L5 ET
ExN L6 IT
ExN L6 CT
ExN L6B
ExN L6 NP
InN CGE
InN MGE
InN dLGE
Astro
Endo
OPC
Oligo
GPC
MG
VLMC
B
Accessible chromatin
C
Age
Midfetal
Late fetal
Cell type
ExN
InN
snRNA
snATAC
−4 −2 0 2 4
D
MEIS2 expression
MA0774.1 motif activity
L3−5IT
L2−3IT
E
Tn5 insertion enrichment
L2−3 IT (PCD 87-96)
L2−3 IT (PCD 104-112)
L2−3 IT (PCD 155)
L3−5 IT (PCD 87-96)
L3−5 IT (PCD 104-112)
L3−5 IT (PCD 155)
Expected Tn5 enrichment
Distance from motif
Bits

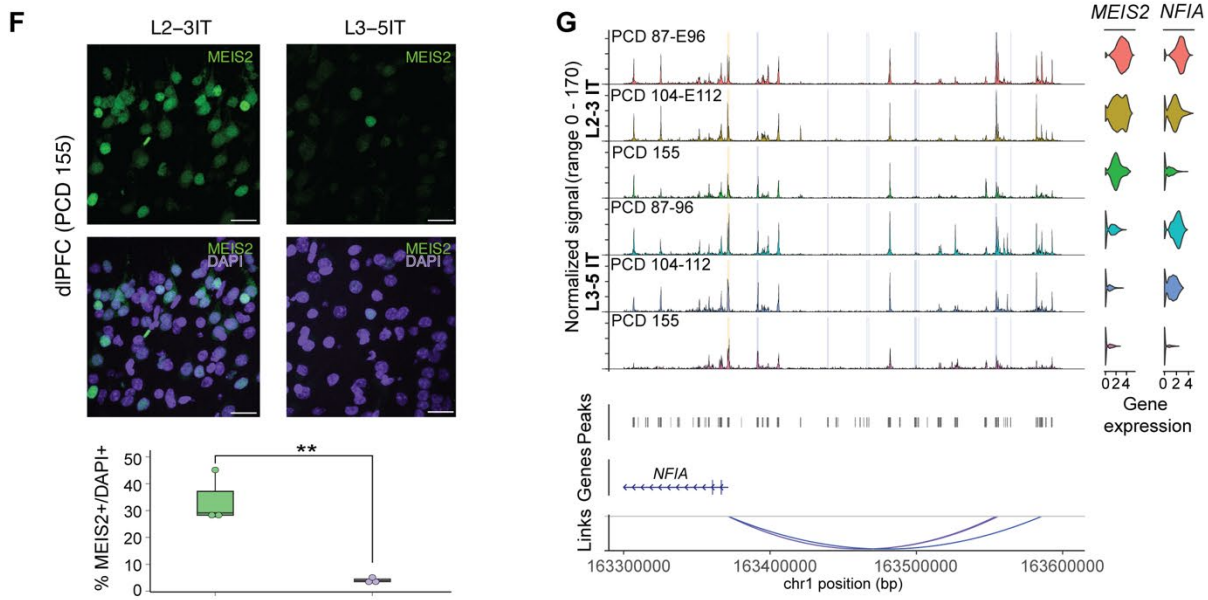
F
L2−3IT
L3−5IT
MEIS2
MEIS2 DAPI
dlPFC (PCD 155)
% MEIS2+/DAPI+
**
L2-3 IT
L3-5 IT
G
PCD 87-E96
PCD 104-E112
PCD 155
PCD 87-96
PCD 104-112
PCD 155
L2-3 IT
L3-5 IT
Normalized signal (range 0 - 170)
MEIS2
NFIA
Gene expression
Peaks
Genes
Links
NFIA
163300000
163400000
163500000
163600000
chr1 position (bp)

Fig. 3. Single-nucleus multiome gene expression and chromatin accessibility of rhesus macaque dlPFC cells across mid-late fetal development

(A) UMAP of all cell subclasses based on gene expression. **(B)** UMAP of all cell subclasses based on chromatin accessibility. **(C)** Heatmap showing gene expression and chromatin accessibility peak profiles corresponding to top gene-to-peak links inferred for excitatory and inhibitory neuronal cell types across mid- and late-fetal developmental stages. Each row indicates an inferred gene-to-peak link and each column indicates a pseudo-cell. **(D)** UMAP visualization of L2-3 IT and L3-5 IT cells; left panel is colored according to *MEIS2* expression; right panel is colored according to motif activity scores for MA0774.1 (MEIS2 transcription factor motif). **(E)** MEIS2 transcription factor footprints for ExN L2-3 IT and ExN L3-5 IT cells across three developmental periods (PCD 87-96, PCD 104-112, and PCD 155). **(F)** Immunfluorescent detection of MEIS2 in the macaque dlPFC at PCD 155, in L2-3 and L3-5 cells; bottom panel shows that a significantly higher number of cells express MEIS2 in L2-3 than in L3-5 (L3-5 was identified using in situ hybridization against *RORB*, as shown in fig. S10C). Scale bar, 20 µm. (**$p < 0.01$, *t*-test) **(G)** Peak-to-gene link plot for *NFIA* together with the gene expression of *MEIS2* and *NFIA* in ExN L2-3 IT and ExN L3-5 IT across three developmental periods. The links indicate the activity links between *NFIA* gene expression and chromatin accessibility peaks. The highlighted regions within the chromatin accessibility peaks show the MEIS2 transcription factor motif (MA0774.1) binding sites. IT, intratelencephalic; ET, extratelencephalic; CT, corticothalamic; NP, near-projecting; CGE, caudal ganglionic eminence; MGE, medial ganglionic eminence; dLGE, dorsal lateral ganglionic eminence; Astro, astrocytes; Endo, endothelial cells; OPC, oligodendrocyte precursor cells; Oligo, oligodendrocytes; GPC, glial precursor cells; MG, microglia; VLMC, vascular leptomeningeal cells.

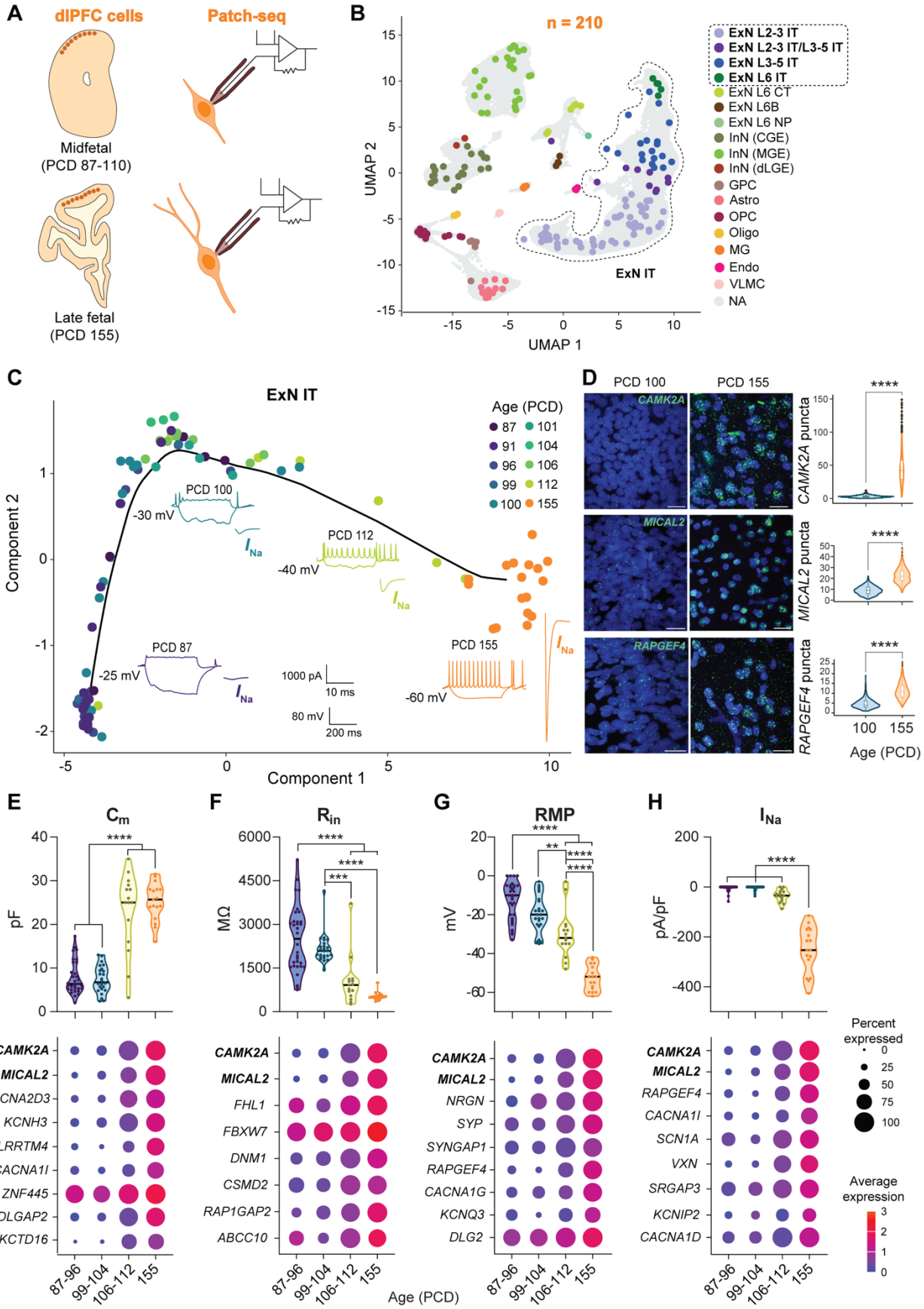
A
dlPFC cells
Patch-seq
Midfetal
(PCD 87-110)
Late fetal
(PCD 155)
B
n = 210
ExN L2-3 IT
ExN L2-3 IT/L3-5 IT
ExN L3-5 IT
ExN L6 IT
ExN L6 CT
ExN L6B
ExN L6 NP
InN (CGE)
InN (MGE)
InN (dLGE)
GPC
Astro
OPC
Oligo
MG
Endo
VLMC
NA
ExN IT
UMAP 1
UMAP 2
C
ExN IT
Age (PCD)
87
91
96
99
100
101
104
106
112
155
PCD 100
-30 mV
PCD 112
-40 mV
PCD 87
-25 mV
PCD 155
-60 mV
1000 pA
10 ms
80 mV
200 ms
Component 1
Component 2
D
PCD 100
PCD 155
CAMK2A
MICAL2
RAPGEF4
CAMK2A puncta
MICAL2 puncta
RAPGEF4 puncta
Age (PCD)
E
Cm
pF
F
Rin
MΩ
G
RMP
mV
H
INa
pA/pF
CAMK2A
MICAL2
CACNA2D3
KCNH3
LRRTM4
CACNA1I
ZNF445
DLGAP2
KCTD16
FHL1
FBXW7
DNM1
CSMD2
RAP1GAP2
ABCC10
NRGN
SYP
SYNGAP1
RAPGEF4
CACNA1G
KCNQ3
DLG2
CACNA1I
SCN1A
VXN
SRGAP3
KCNIP2
CACNA1D
87-96
99-104
106-112
155
Age (PCD)
Percent expressed
Average expression

Fig. 4. Identification of midfetal and late fetal primate neuronal maturation-related genes using Patch-seq

(A) Schematic representation of the Patch-seq experimental design for analyzing midfetal and late fetal rhesus macaque dlPFC cells. **(B)** Integration of the 210 cells profiled by Patch-seq onto the snRNA-seq reference UMAP. **(C)** Pseudotime trajectory based on the gene expression profiles of patched IT neurons from 14 individual rhesus macaque fetal brains at 10 distinct fetal ages, with representative electrophysiological sample traces (voltage responses to depolarizing and hyperpolarizing current injections, and inward sodium currents) that demonstrate neuronal maturation across fetal development. **(D)** In situ hybridization detection and quantification (right panel) of *CAMK2A*, *MICAL2*, and *RAPGEF4* in PCD100 and PCD155 rhesus macaque fetal cortical brains. Scale bar, 20 µm. (****$p < 0.0001$, *t*-test). **(E-H)** Plots illustrating the developmental changes in various electrophysiological properties, including **(E)** membrane capacitance (C_m), **(F)** input resistance (R_{in}), **(G)** resting membrane potential (RMP), and **(H)** inward sodium current (I_{Na}), of IT neurons across four different age groups. Bottom panels show the expression levels of **(E)** C_m-correlated genes, **(F)** R_{in}-correlated genes, **(G)** RMP-correlated genes, and **(H)** I_{Na}-correlated genes in IT neurons across the same age groups. (**$p < 0.01$, ***$p < 0.001$, ****$p < 0.0001$, one-way ANOVA, Tukey's multiple comparisons test). ExN, excitatory neurons; IT, intratelencephalic; ET, extratelencephalic; CT, corticothalamic; NP, near-projecting; InN, inhibitory neurons; CGE, caudal ganglionic eminence; MGE, medial ganglionic eminence; dLGE, dorsal lateral ganglionic eminence; GPC, glial precursor cells; Astro, astrocytes; OPC, oligodendrocyte precursor cells; Oligo, oligodendrocytes; MG, microglia; Endo, endothelial cells; VLMC, vascular leptomeningeal cells.

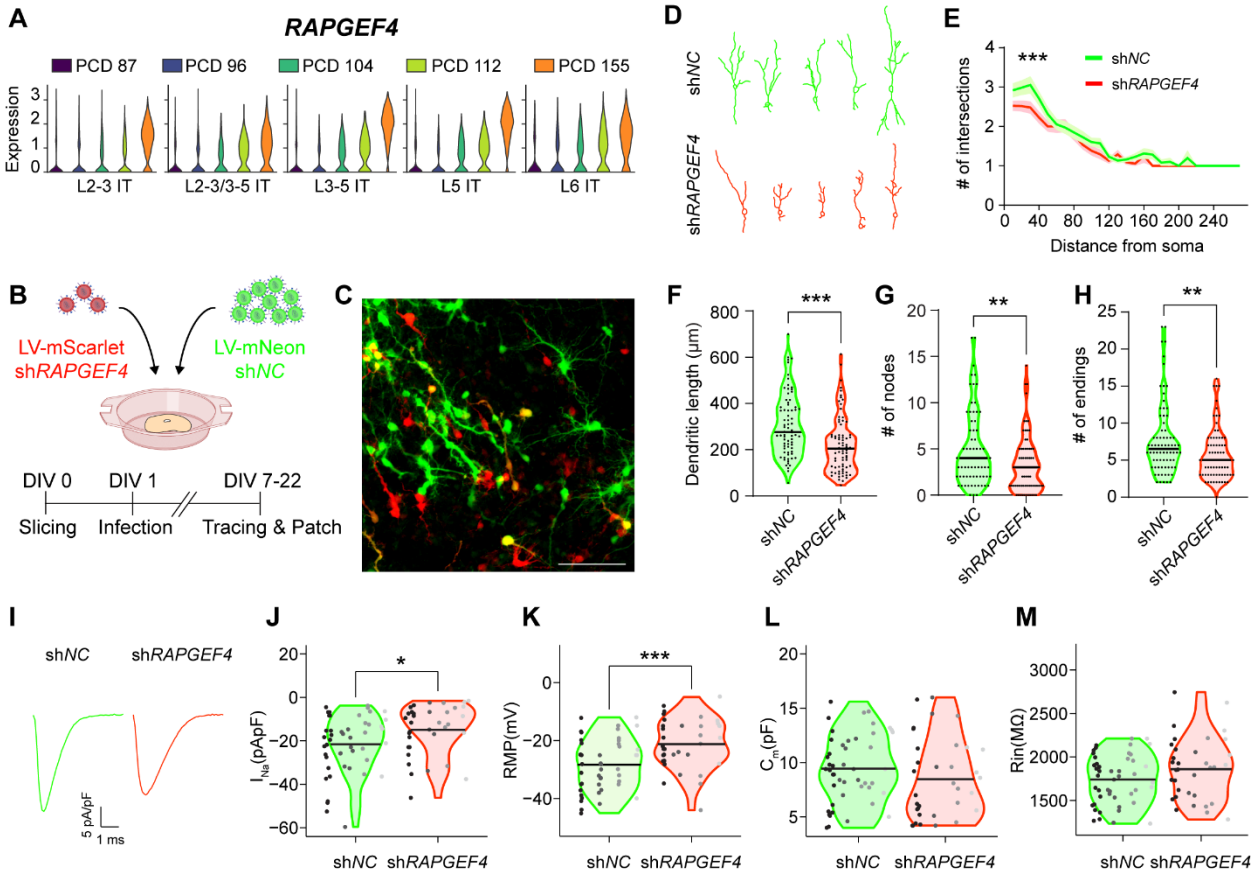

Fig. 5. Knockdown of RAPGEF4 impairs morphological and electrophysiological maturation of cortical neurons in macaque organotypic dlPFC slices

(A) Violin plots showing the expression of *RAPGEF4* in IT neurons in rhesus macaque dlPFC from PCD87 to PCD155. **(B)** Schematic of the experimental setup used to investigate the morphological and electrophysiological alterations after *RAPGEF4* knockdown in ex vivo rhesus macaque fetal dlPFC slices. **(C)** Confocal microscopy image depicting *RAPGEF4* knockdown (mScarlet+(red), mScarlet+ and mNeon+(yellow)) and control (mNeon+(green only)) neurons in macaque dlPFC slices. Scale bar, 100 µm. **(D)** Sample traces show the morphology of both *RAPGEF4* knockdown (bottom panel) and control (top panel) neurons. **(E)** Dendritic complexity is decreased in *RAPGEF4* knockdown neurons compared to control neurons [$F(1,150) = 14.531$, ***$p < 0.001$, multivariate analysis of variance (MANOVA)]. Knockdown of *RAPGEF4* decreases **(F)** total dendritic length, **(G)** number of nodes, and **(H)** number of endings (*t*-test, ***$p < 0.001$, **$p < 0.01$). (I) Representative inward sodium current traces for *RAPGEF4*

knockdown (right panel) and control (left panel) neurons. **(J-M)** Knockdown of *RAPGEF4* increases **(J)** I_{Na} and **(K)** RMP, but does not change **(L)** C_m and **(M)** R_{in} (*t*-test, ***$p < 0.001$, *$p < 0.05$).

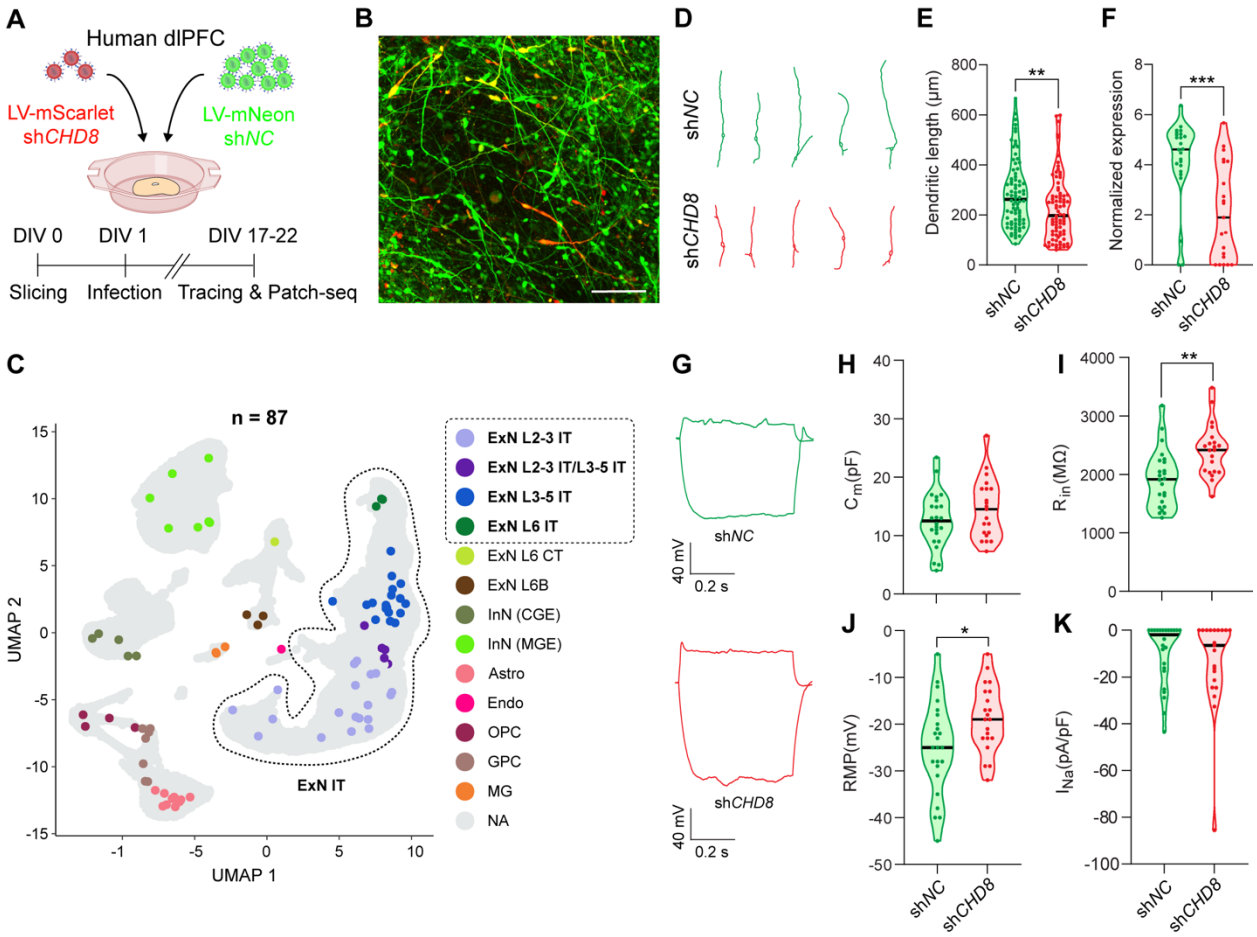

Fig 6. Knockdown of *CHD8* impairs maturation of cortical excitatory neurons in human organotypic dlPFC slices

(A) Schematic diagram illustrating the experimental setup used to study the morphological and electrophysiological changes after knockdown of *CHD8* in ex vivo human fetal cortical slices. **(B)** Confocal microscopy image showing *CHD8* knockdown (mScarlet+(red), mScarlet+ and mNeon+(yellow)) and control (mNeon+(green only)) neurons in human cortical slices. Scale bar, 100 µm. **(C)** Integration of the 87 human cells profiled by Patch-seq onto the snRNA-seq reference UMAP. **(D)** Sample traces demonstrating the morphology of both *CHD8* knockdown and control neurons. **(E)** *CHD8* knockdown reduces total dendritic length (**$p < 0.01$, *t*-test). **(F)** Expression of *CHD8* in IT neurons from human ex vivo slices (***$p < 0.001$, *t*-test). **(G)** Representative traces (voltage response to depolarizing [50 pA] and hyperpolarizing [-50 pA] current injections) for *CHD8* knockdown and control neurons. **(H-K)** *CHD8*

knockdown increases **(I)** R_{in} and **(J)** RMP, but does not alter **(H)** C_m and **(K)** I_{Na} (*$p < 0.05$, **$p < 0.01$, *t*-test).